Energy conversion of biomass char: Oxidation rates in mixtures of O2/CO2/H2O

Karlström, Oskar; Hupa, Leena

Published in:
Energy

DOI:
10.1016/j.energy.2019.05.192

Published: 01/01/2019

Document Version
Accepted author manuscript

Document License
CC BY-NC-ND

Energy conversion of biomass char: oxidation rates in mixtures of $O_2/CO_2/H_2O$

O. Karlström, L. Hupa

Johan Gadolin Process Chemistry Centre, Åbo Akademi University, Turku, Finland

***corresponding author, email:** okarlstr@abo.fi, phone: +358 2 215 3275

Abstract

In thermal energy conversion of biomass, the char conversion rate influences the design of industrial systems. Yet there is no consensus on the relative influences of O_2, CO_2 and H_2O on the char conversion rate. The present study aims at clarifying the roles of these oxidizers on biomass char conversion. Single particles of different particles sizes were oxidized in mixtures of O_2/N_2, CO_2/N_2, H_2O/N_2 and $O_2/CO_2/H_2O/N_2$ at various temperatures. The results show that for large particles and high temperatures, CO_2 and H_2O gasification reactions play a dominant role, while for sufficiently small particles and low temperatures, the O_2 oxidation reaction plays a dominant role in mixtures of $O_2/CO_2/H_2O/N_2$. Two different particle models were used to compute char conversions: a detailed single particle model, and a conventional particle model assuming that rates in mixtures of oxidizers can be predicted based on rates of single oxidizers. The results show that the char oxidation rates are strongly overestimated when predicting rates based on single oxidizers, while the detailed model shows a good agreement to the experimental measurements.

Keywords: biomass, char, oxidation, combustion, gasification

1. Introduction

In thermal conversion of solid biomass, a fuel particle undergoes drying and devolatilization, forming a char residue. The char carbon (char-C) is oxidized by O_2, CO_2 and H_2O. The conventional hypothesis is that the char carbon reacts with oxygen and that the reactions between CO_2 and H_2O can be neglected under most combustion conditions. For coal chars, however, it has been suggested that also the reactions with CO_2 and H_2O are important at the high temperatures typical for pulverized fuel combustion [1]. Khitrin [2] showed, by combining effects of chemical kinetics and diffusion, that gasification by CO_2 and H_2O becomes significant at around 1300-1500 °C for low reactivity coal chars and particle sizes larger than 2 mm. Stanmore and Visona [3] concluded that gasification by CO_2 and H_2O contribute slightly to carbon burnout under conditions for pulverized coal combustion. Hecht et al. [4] used a detailed mathematical particle model, which showed that gasification reactions may account for 20-30% of the total char carbon conversion at around 1400 °C. Biomass chars are often very reactive [5] and, in general, several magnitudes more reactive than coal chars towards CO_2 and H_2O [6]. As a result, it can be expected that the heterogeneous gasification reactions become significant at lower temperatures for biomass chars than for coal chars.

Char carbon reactions with either O_2, CO_2 or H_2O have been investigated in numerous studies (see for example review studies [1,6]). The reaction between char-C and CO_2, for example, can be expressed by the following mechanism [7]:

$C + CO_2 \rightleftharpoons C(O) + CO(g)$ (R1)

$C(O) \rightarrow CO$ (R2)

Here C(O) is a carbon-oxygen surface complex [8], which has been investigated in detail [9]. The dissociation reaction (R1) is accelerated due to a redox cycle [10] involving catalytic species such as Ca and K [11]. Such catalytic gasification can be expressed by the following mechanism [12]:

$CO_2 + * \rightleftharpoons CO + O*$ (R3)

$O* + C_f \rightleftharpoons C(O) + *$ (R4)

$C(O) \rightarrow CO$ (R5)

where [*] represents the "empty" and oxygen containing metal species active for oxygen transfer to a free carbon site C_f resulting in a carbon-oxygen surface complex C(O). The reactions between C and H_2O or O_2 can be expressed in an equivalent way [13].

The kinetics of the reactions between char-C and CO_2 or H_2O are significantly slower than the kinetics of the reaction between char-C and O_2 [2]. The reaction between O_2 and biomass char-C is so rapid that it can be assumed mass transfer limited (Regime III) under most combustion conditions, i.e., a sufficiently large particle size and at high temperatures. The reactions between char-C and CO_2 and H_2O occur under conditions limited by the combined effects of chemical kinetics and pore diffusion (Regime II) for large wood char particles already at 800 °C [14-17]. The simultaneous reactions between char-C and O_2, H_2O and CO_2 have been investigated for coal chars under kinetically limited conditions (Regime I) (e.g. [2,3]). Yet, no study has investigated biomass char-C conversion in various mixtures of $O_2/CO_2/H_2O/N_2$ under well-controlled conditions. Models for char conversion in mixtures of $O_2/CO_2/H_2O/N_2$ are needed in order to predict the contributions of the different oxidizing species on char conversion, which influence the reaction rate [2], the particle temperature [4] and other critical factors such as the fate of the char bound nitrogen [18]. The char-N reacts differently with O_2, H_2O and CO_2 [19] and, thus, the final nitrogen emissions cannot be predicted without considering effects of CO_2 and H_2O on char conversion. In addition, it is of great importance to understand the reaction rates in the design of combustion and gasification systems, since the char conversion is the slowest conversion step [20]: it is important that the char conversion is as complete as possible, so that the ash has a sufficiently low carbon content [21].

The present study investigates biomass char conversions in various mixtures of $O_2/CO_2/H_2O/N_2$. Single particles with a diameter of 8 and 10 mm were combusted in mixtures of O_2/N_2, CO_2/N_2, H_2O/N_2 and $O_2/CO_2/H_2O/N_2$ at 800, 850 and 900 °C. Computed and experimental char conversions are compared in order to clarify the roles of O_2, CO_2 and H_2O. In addition, it is investigated whether oxidation rates in mixtures of oxidizers can be predicted directly based on oxidation rates occurring with single oxidizers.

2. Methods

2.1 Model formulation

The model presented here is based on the model by Karlström et al. [22]. The following reaction mechanism is used to model the char-C reactions with O_2, H_2O and CO_2:

$C + C + O_2$	$\rightarrow C(O) + CO$	S1
$C(O)$	$\rightarrow CO$	S2
$C + CO_2$	$\leftrightarrow C(O) + CO$	S3
$C(O)$	$\rightarrow CO$	S4
$C + H_2O$	$\leftrightarrow C(O) + H_2$	S5
$C(O)$	$\rightarrow CO$	S6

In this study, S2, S4 and S6 are modeled as separate reactions. The reaction rate constant K_i (mol/m^{3}s) for char consumption by species *i* can be expressed in a Langmuir-Hinshelwood form (exemplified for CO_2) as

$$K_{CO_2} = c_{CO_2} k_{ads,CO_2} \frac{1}{1 + \frac{k_{ads,CO_2}}{k_{des,CO_2}} c_{CO_2}} \quad (1)$$

where $k = Ae^{-E/RT}$ is an Arrhenius rate; E is the activation energy (kJ/mol); and A is the pre-exponential factor (1/s for A_{ads}, mol /(s·m^3) for A_{des}). S3 is modeled as a lumped reaction in the forward direction. The hydrogen inhibition on steam gasification, i.e., the backward direction of S5 is taken into consideration due to the high hydrogen concentrations in the experiments. Oxidation of CO to CO_2 and reactions involving CO, H_2, H_2O and CO_2 are taken into consideration using the global Howard mechanism [23] and the Jones-Lindstedt [24] mechanism, respectively.

The char particle is assumed spherical and divided into q layers (q=40 in the study). In a layer *w* in the particle, the char conversion, X_w, is given as

$$X_w = 1 - \frac{n_{C,w}}{n_{C,0}} \quad (2)$$

at a given time. The total char-C conversion is defined as

$$X = 1 - \frac{n_{C,total}}{n_{C,total,0}} \quad (3)$$

where n_C is the amount of carbon; *0* is initial; and *total* refers to the total amount of carbon in all layers. As the degree of conversion in one layer exceeds 0.999, the layer disappears and, as a result, the particle shrinks and ash remains. The amount of carbon is given by

$$n_{C,w}(t) = n_{C,w}(t - \Delta t) + \Delta t \cdot \dot{n}_{C,w} \quad (4)$$

The char gasification rate can be expressed as

$$\dot{n}_{C,w} = V_w \dot{n}'''_{C,w} \quad (5)$$

Here V is the volume of layer w (m^3); and $\dot{n}'''_{C,w}$ refers to char-C consumption rate (mol/m^3s) in layer w and can be expressed, exemplified for CO_2, as

$$\dot{n}'''_{C,w} = -\Omega f(X_w) K_{CO_2} \quad (6)$$

Here Ω is a stoichiometric ratio; K_i is the reaction rate constant for char consumption by species i and $f(X)$ is the surface function. $f(X)$ is defined in the following way: at any degree of conversion, X, the surface function is defined as the rate occurring under kinetically limited conditions divided by the initial rate ($X = 0$) occurring under kinetically limited conditions. Thus for $X = 0$, $f(X) = 1$ and for $0 < X < 1$, $f(X) > 0$.

Concentrations and the temperature in the particle and in the boundary layer are computed from

$$\frac{1}{S(r)} \frac{d}{dr} \left(S(r) D_j \frac{dc_j}{dr} + U c_j S(r) \right) = \dot{n}'''_j \quad (7)$$

and

$$\frac{1}{S(r)} \frac{d}{dr} \left(S(r) \lambda \frac{dT}{dr} \right) + \frac{1}{S(r)} \frac{d}{dr} \left(\sum_{i=1}^{i_{max}} \dot{n}_i H_i \right) = \sum_{j=1}^{j_{max}} \dot{n}'''_j H_j \quad (8)$$

Here $S(r)$ is the surface area of a sphere with the radius r; c is the concentration (mol/m^3); U is the velocity of gases flowing; inside the particle λ is the effective thermal conductivity of the solid particle and outside the particle λ is the mixture-averaged gas thermal conductivity (W/mK); and H_j is the specific enthalpy of a gas species (J/mol). The effective thermal conductivity was estimated following Thunman et al. [25]. Effects of the heterogeneous and homogeneous reactions are incorporated in $\dot{n}'''_j$ which is the consumption or production rate of species (mol/m^3s). In Eq. 7 and 8, the second term on the left-hand side accounts for effects of the Stefan flow. D_j (m^2/s) equals the diffusion coefficient for species j in a multicomponent gas mixture. The diffusion coefficient is calculated based on [26]:

$$D_j = \frac{\Phi}{2} D_{j,\infty} \quad (9)$$

where Φ is the porosity.

At the external surface, the heat transfer is calculated by convection and conduction according to Eq. 8 and by radiation. Radiation heat transfer (J/s) is calculated as

$$\dot{Q}_{rad} = S_e \sigma \varepsilon \left(T_{rad}{}^4 - T_p{}^4 \right) \quad (10)$$

Here S_e is external surface area of the particle; σ is the Stefan-Boltzmann constant ($5.67 \cdot 10^{-8}$ $Wm^{-2}K^{-4}$); ε is surface emissivity, here set to 0.6 [27]; and T_{rad} is the radiation temperature. The radiation temperature is assumed equal the temperature of the furnace walls. The radiation is computed by considering a small convex object in a large enclosure. The apparent one-dimensional boundary layer thicknesses for the concentration, $\delta_{m,j}$, and temperature δ_h, are defined as

$$\delta_{m,j} = \frac{d_p}{Sh_j - 2} \quad (11)$$

and

$$\delta_h = \frac{d_p}{Nu - 2} \quad (12)$$

where d_p is particle diameter (m); *Sh* is the Sherwood number; and *Nu* is the Nusselt number.

The boundary conditions for Eq. 7 and 8 are at r = 0:

$\frac{dc_i}{dr} = 0$, (12) $\frac{dT}{dr} = 0$, (13) at $r = R + \delta_{m,j}$, $c_j = c_{j,\infty}$ (14) and at $r = R + \delta_h$ $T = T_\infty$ (15)

2.2 Experiments with single oxidants to determine kinetic parameters

2.2.1 Materials

The biomass investigated was pine wood (softwood). Elemental analysis of the biomass and the char is shown in Table 1. Single particle samples were prepared by pressing 200 mg and 500 mg of biomass into cylindrical pellets with a diameter of 8 mm and 10 mm, respectively. A single pellet is hereafter referred to as a single particle. These particle sizes are in the range of particle sizes in, for example, fluidized bed combustion of biomass [28].

Table 1. Elemental analysis of the biomass and of the char.

Biomass fuel	wt-% of dry biomass				wt-% of char		
	N	**C**	**H**	**S**	**N**	**C**	**H**
Softwood	0.14	50.20	6.27	0.005	0.17	92.05	0.44

2.2.2 Single particle reactor

Char conversion experiments were conducted in a single particle reactor at 800, 850 and 900 °C in mixtures of O_2/N_2, CO_2/N_2, H_2O/N_2 and $O_2/CO_2/H_2O/N_2$. Table 2 lists the different conditions. Figure 1 shows the single particle reactor. A detailed description and a schematic picture of the reactor can be found elsewhere [29]. Gas mixtures were fed to the bottom of the reactor (which has a diameter of 44.3 mm) and the product gases left the reactor from the top of the reactor. The ratio cross-sectional surface area / superficial area of particle is > 20, and the ratio reactor volume / particle volume is > 700. The biomass sample was inserted into the reactor using a movable probe that could be inserted from room temperature into the hot reactor within one second. The movable probe with the sample holder was horizontally inserted into the reactor. The sample holder consisted of a thin Pt net on which a single fuel pellet was placed. Under the investigated conditions, the superficial gas velocity in the reactor is ~0.15 m/s, giving a Reynolds number for the flow in the reactor of around 40 and a Reynolds number for the flow around the initial particle to around 10.

Table 2. Experimental conditions in single particle reactor.

no	**d (mm)**	**T (°C)**	**O_2***	**CO_2**	**H_2O**	***no***	**d (mm)**	**T (°C)**	**O_2**	**CO_2**	**H_2O**
1	8	800	3	0	0	*21*	8	900	0	0	14
2	8	800	6	0	0	*22*	8	900	0	0	34
3	8	850	3	0	0	*23*	10	850	0	0	14
4	8	850	6	0	0	*24*	10	850	0	0	34
5	8	900	3	0	0	*25*	8	800	0	17	14
6	8	900	6	0	0	*26*	8	800	0	34	14
7	10	850	3	0	0	*27*	8	800	3	34	14
8	10	850	6	0	0	*28*	8	800	6	34	14
9	8	800	0	17	0	*29*	8	850	0	17	14
10	8	800	0	34	0	*30*	8	850	0	34	14
11	8	850	0	17	0	*31*	8	850	3	34	14
12	8	850	0	34	0	*32*	8	850	6	34	14
13	8	900	0	17	0	*33*	8	900	0	17	14
14	8	900	0	34	0	*34*	8	900	0	34	14
15	10	850	0	17	0	*35*	8	900	3	34	14
16	10	850	0	34	0	*36*	8	900	6	34	14
17	8	800	0	0	14	*37*	10	850	0	17	14
18	8	800	0	0	34	*38*	10	850	0	34	14
19	8	850	0	0	14	*39*	10	850	3	34	14
20	8	850	0	0	34	*40*	10	850	6	34	14

*vol.%

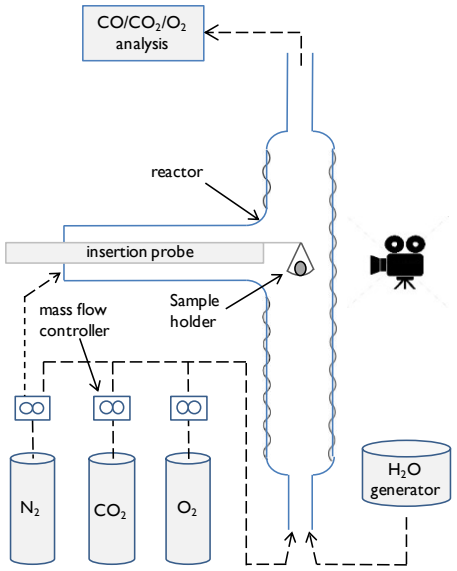

Fig. 1. Åbo Akademi Single particle reactor.

2.2.3 Char conversions

Concentrations in the outlet gases were continuously measured using a non-dispersive infrared analyzer (ABB AO2020) for CO and CO_2 and a paramagnetic analyzer for O_2. Fig. 2 exemplifies a char gasification test of a single pellet at 900 °C and 17% CO_2. In the example given above, the devolatilization is given by the peak close to the x-axis (concentration of CO) on the left hand side. After devolatilization, gasification of the char residue started, which is the objectives of the present study. By integrating and normalizing the char gasification part from the left-hand side of Fig. 2, an experimentally-derived char gasification curve is obtained. This experimentally-derived char gasification profile, hereafter called char conversion, is shown on the right-hand side of Fig. 2. Note that the char gasification is defined to start at 0 s on the right-hand side.

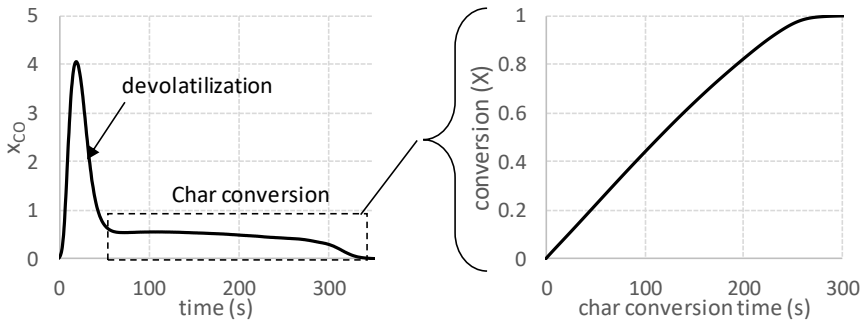

Fig. 2. Left: measured concentrations of CO at 900 C and 17 % CO_2. Right: char conversion based on the measured data on the left-hand side.

In the end of the devolatilization, the time derivatives of the measured CO signal decreased rapidly, followed by a steep increase in the derivative. The local minimum of the derivatives is defined as the starting point of the char gasification. The end point of the char conversion is defined as when CO is not released anymore from the particle. In the experiments with H_2O and O_2, also concentrations from the CO_2 and O_2 analyzers were considered when determining the char conversions.

After the devolatilization, the particle shape had changed from cylindrical to a cylinder, with an aspect ratio close to one, with rounded edges. During the conversion, the shape changed and became more and more spherical. For simplicity, the particle is assumed spherical in the modeling. Initially it is estimated that, due to the assumption of a sphere, that the external surface area is underestimated by around 20%, and the mass transfer of gases to the particle is underestimated by less than 10%. In the experiments, the 8 mm particle with the initial mass of 200 mg formed a char particle with a diameter of approximately 8 mm, while the 10 mm particle with the initial mass of 500 mg formed a char particle with a diameter of approximately 10 mm.

In the results section the term char gasification time is used. This is the time between when the char gasification starts and when the char has been consumed. The error margin for the char gasification times of the experiments were determined to 2 seconds (error margin from the onset of char gasification) + the standard deviation at a given condition, which was generally below 2% of the total conversion times. In general, the experiments were repeated three times.

2.2.4 Determination of kinetic parameters

The kinetic parameters for the heterogeneous reactions by CO_2 and H_2O were determined based on fitting computed and experimental char conversions, such as the char conversion shown in Fig. 2, using a multivariable optimization method [30]. The reactions between O_2 and char-C were assumed mass transfer limited. The kinetic parameters were determined by minimizing the residuals between the computed and experimental char conversions according to the least-squares objective function:

$$f_{min} = \left(\frac{1}{v_{max} z_{max}} \sum_{v} \sum_{z} f_{v,z}^2 \right)^{1/2}, \qquad (16)$$

where

$$f_{v,w} = \left(X_{mod} - X_{expt} \right)_{v,z}. \qquad (17)$$

Here, the subscript *mod* stands for modeled and *exp* for measured; v,z refers to the v^{th} point of the experimentally-derived char conversion for the z^{h} experimental test condition.

2.3 Validation of model in mixtures of $O_2/CO_2/H_2O/N_2$

Using the determined kinetic parameters, the model was used to compute char conversions in mixtures of $O_2/CO_2/H_2O/N_2$. The char conversions were validated by single particle experiments similar to the ones described in section 2.2. The investigated conditions are listed in Table 2.

3. Results and discussion

3.1 Char conversion in O_2/N_2, CO_2/N_2 and H_2O/N_2

Table 3 lists the determined kinetic parameters. The activation energies are in agreement to previously reported values (see for example Review study [1]). Fig. 3 shows computed and experimental char conversions in CO_2/N_2, H_2O/N_2 and O_2/N_2. It can be seen that the computed and experimental char conversions are in good agreement for CO_2/N_2 and H_2O/N_2 under the investigated conditions. In addition, the good agreement between the computed and experimental char conversions in O_2/N_2 implies that the char oxidation is mass transfer limited. The figure shows that the char is slightly more reactive towards H_2O than CO_2, but significantly more reactive towards O_2, as expected.

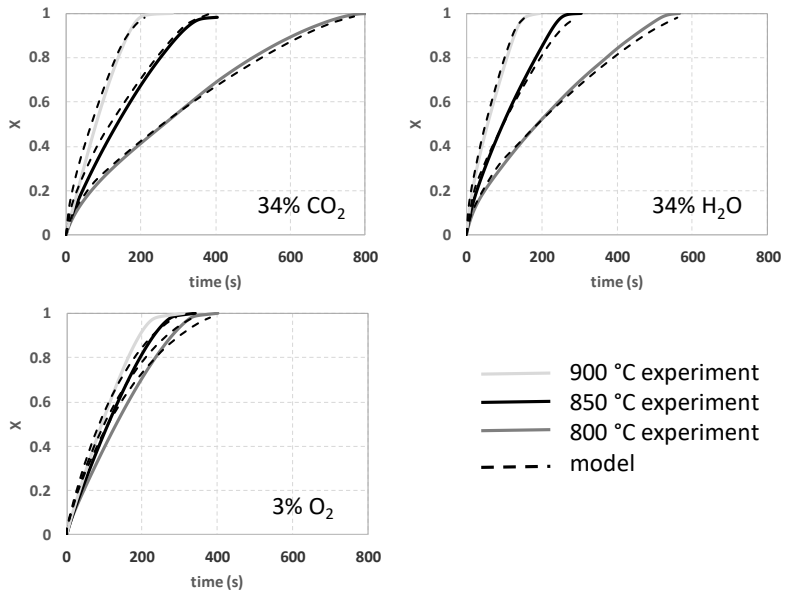

Fig. 3. Computed and expt char conversions with 34% CO_2, 34% H_2O or 3% O_2.

Table 3. kinetic parameters

$A_{ads,\ CO2}$	3.54e+09±2.82 e+08*
$E_{ads,\ CO2}$	176***
$A_{des,\ CO2}$	8.43e+10±6.74 e+09 **
$E_{des,\ CO2}$	184
$A_{ads,H2O}$	6.64e+09±5.31 e+08
$E_{ads,H2O}$	176
$A_{des,H2O}$	8.43e+10±6.74 e+09
$E_{des,H2O}$	184
$A_{ads,O2}$	(→∞)
$E_{ads,O2}$	1
$A_{des,O2}$	(→∞)
$E_{des,O2}$	1
$A_{H2,inhibition}$	4.43e+11
$E_{H2,inhibition}$	200

***A_{ads} (1/s)**
****A_{des} (mol /(s·m^3)**
*****E (kJ/mol)**

3.2 Char conversion in mixtures of $H_2O/CO_2/O_2/N_2$

Fig. 4 plots computed and experimental char conversions in a mixture of $O_2/CO_2/H_2O/N_2$ at 800, 850 and 900 °C for an 8 mm char particle and at 850 °C for a 10 mm char particle. In general, the computed and experimental conversions are in good agreement. At 800 °C, the computed char conversion is slightly more rapid than the experimental char conversion. This can be explained by several factors. For example, the global homogenous chemistry mechanism may be invalid at too low temperatures as suggested by Saastamoinen et al. [31]. Also, the CO_2 and H_2O gasification reactions may compete for the same available carbon active sites [1,32,33]. Interestingly, the computed char conversions in $CO_2/H_2O/N_2$, i.e., without O_2, at 800 °C are slightly slower than the corresponding experimental char conversions (see supplementary material), implying that CO_2 and H_2O are not competing for the same surface area. Nevertheless, in general the agreements between the computed and experimental char conversions are good, implying that the modeling assumptions are reasonable under the investigated conditions. All computed and experimental char conversion times for the investigated conditions are given in the supplementary material.

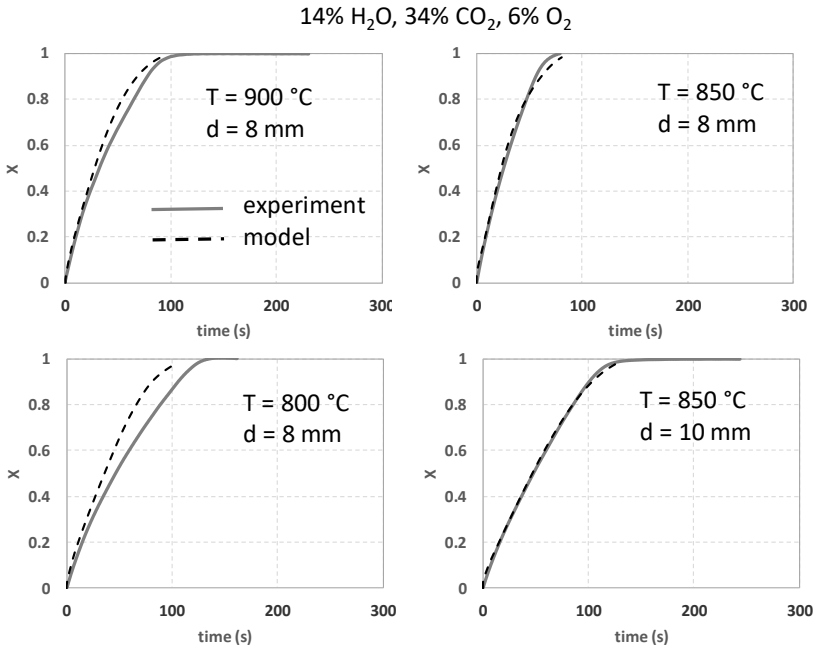

Fig. 4. Computed and experimental char conversions at 800, 850 and 900 °C for an 8 mm char particle and 850 °C for a 10 mm char particle in a mixture of $CO_2/H_2O/O_2$.

The figure shows that the char conversion is slower for the larger particle size. This was consistent for all the investigated conditions with different particle sizes. In general, it can be expected that, under Regime III conditions, the char conversion rate is proportional to the external surface area times the mass transfer coefficient, which is proportional to the inverse diameter. Thus, the char conversion rate is approximately proportional to the diameter of the particle under Regime III conditions. Under Regime I conditions, the instantaneous char conversion rate does not depend on the particle size. Under Regime II conditions, it can be expected that the char conversion rate is less dependent on the particle size than under

Regime III conditions. Since the char conversion time depends on the diameter in the gasification experiments, it can be concluded that the gasification is not occurring under Regime I conditions

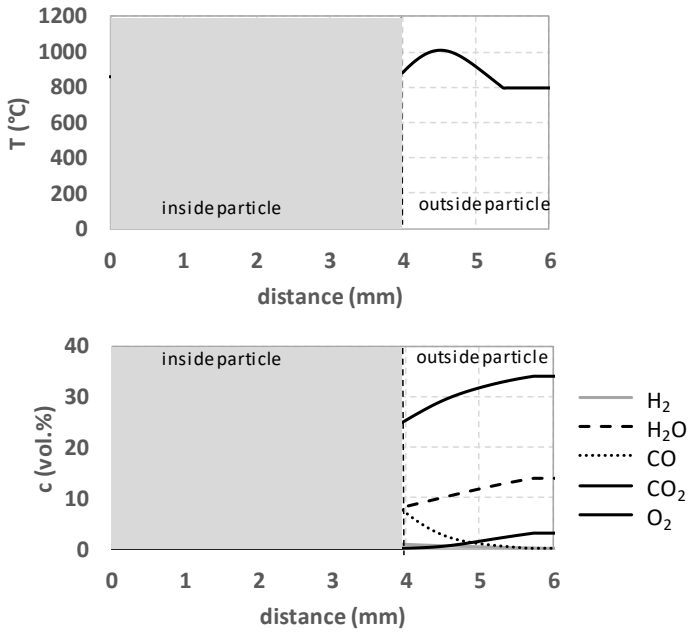

Fig. 5. Computed concentration and temperature profiles for an 8 mm biomass char particle undergoing conversion in a mixture of $CO_2/H_2O/O_2$.

Char conversions in mixtures of $O_2/CO_2/H_2O/N_2$, i.e., at typical combustion or gasification conditions, must be interpreted with caution, since many phenomena occur simultaneously. Fig. 5 illustrates computed temperature gradients and concentration gradients inside and in the boundary layer of the 8 mm particle combusted in a mixture of $O_2/CO_2/H_2O/N_2$ at 800 °C. A steep rise in temperature can be observed outside the particle. This can be explained by the oxidation of CO to CO_2. This homogeneous oxidation reaction consumes oxygen and, thus, the incoming flow of oxygen to the particle surface decreases. Inside the particle, concentration gradients of both H_2O and CO_2 can be observed, which can be explained by pore diffusion resistance. The H_2 concentrations are lower than those of for example CO, which can be explained by the higher diffusion rate of H_2 as compared to the other species. Interestingly, according to the computations, the particle temperature is only slightly higher than the gas temperature, although the reaction rates are very rapid. This can be explained by the occurrence of the endothermic heterogeneous gasification reactions.

In Fig. 5, it can be observed that the oxygen concentration approaches zero in the proximity of the particle surface, which is expected because of mass transfer limitation reasons. In order to determine the relative contribution of O_2, CO_2 and H_2O on the char carbon conversion, one possibility could be to use various isotopes of gas species, i.e., a strategy which previously has been applied in combustion research [34]. Such a sophisticated strategy was out of the scope of the present study and, consequently, the model was used to determine the relative contributions of O_2, CO_2, and H_2O.

3.3 Biomass vs. coal: contributions of O_2, CO_2 and H_2O

Fig. 6A shows the contributions of O_2, CO_2 and H_2O on char conversion at 800 °C in a mixture of O_2, CO_2 and H_2O. In the figure, also the char conversion is shown for the same conditions (Fig. 6B). Initially, the char is gasified entirely by CO_2 and H_2O. However, as the char conversion proceeds, also O_2 begins oxidizing the char. As the conversion proceeds, the role of O_2 becomes increasingly important and, at final char conversion stages, more than 80% of the char carbon consumption can be attributed to char oxidation by O_2. The change in the role of O_2 can be explained by the following: initially the CO_2 and H_2O gasification rates are so rapid that sufficiently high amounts of CO and H_2 are produced, consuming the O_2 in the boundary layer of the particle. After around 20 seconds, there is more O_2 present than what the homogenous oxidation reactions require, and a part of the O_2 reaches the particle surface.

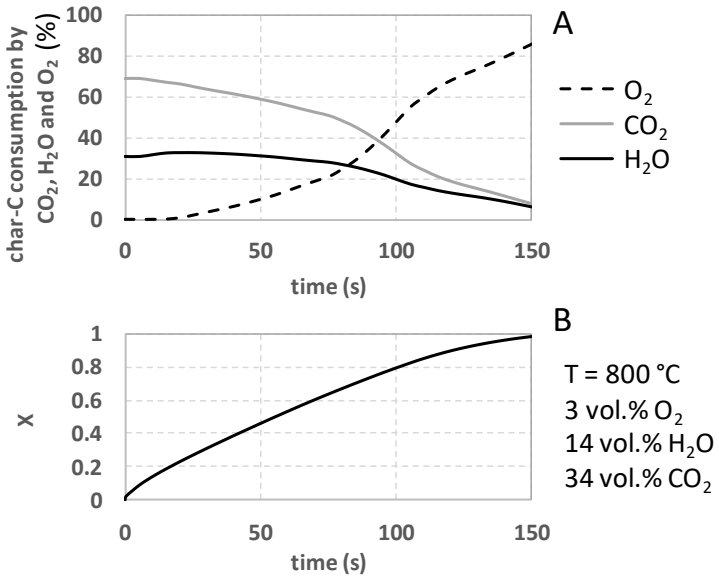

Fig. 6A. Computed char consumption by O_2, CO_2 and H_2O and (B) conversion in a mixture of $CO_2/H_2O/O_2$ at 800 °C.

The model is based on sound kinetic and mass transfer descriptions and, consequently, it is motivated to test the model for other conditions than those experimentally investigated in the present study. In order to assure the accuracy at other conditions, the model must be validated by means of additional experiments, which is out of the scope of the present study. Thus, the corresponding computations were repeated for 1 and 10 mm char particles at 800, 1000 and 1200 °C in a mixture of 5% O_2, 15% CO_2 and 15% H_2O. In industrial combustion systems, the concentrations of O_2, CO_2 and H_2O vary during the char conversion stage, but in many cases it can be expected that the char conversion occurs in an atmosphere with significantly less than 21% O_2, and that CO_2 and H_2O concentration in the gas are significantly higher than the O_2 concentration (see for example [4,35,36]). Fig. 7 shows contributions of O_2, CO_2 and H_2O under these conditions, when the degree of char conversion is 50%. The figure shows that both the size and temperature strongly influence the extents to which O_2, CO_2 or

H_2O convert the char carbon. In general, for large particles and high temperatures, the gasification reactions by CO_2 and H_2O play a dominant role, while for a sufficiently small particle and low temperature, the O_2 oxidation reaction plays a dominant role. In addition, Fig. 7 presents predictions for coal char particles of 1 and 10 mm. In these computations, it is assumed that the pre-exponential factors for the coal char are 0.001 times the pre-exponential factors of the biomass char, giving a relatively reactive coal char. Due to the lower reactivity of coal chars, the O_2 reactions are more dominant than for biomass char. Even at 1200 °C, the reactions with O_2 are dominant for coal char, thus, in contrast to the biomass char. These coal char results are in line with results reported by Khitrin [2], Stanmore and Visona [3] and Hecht et al [4].

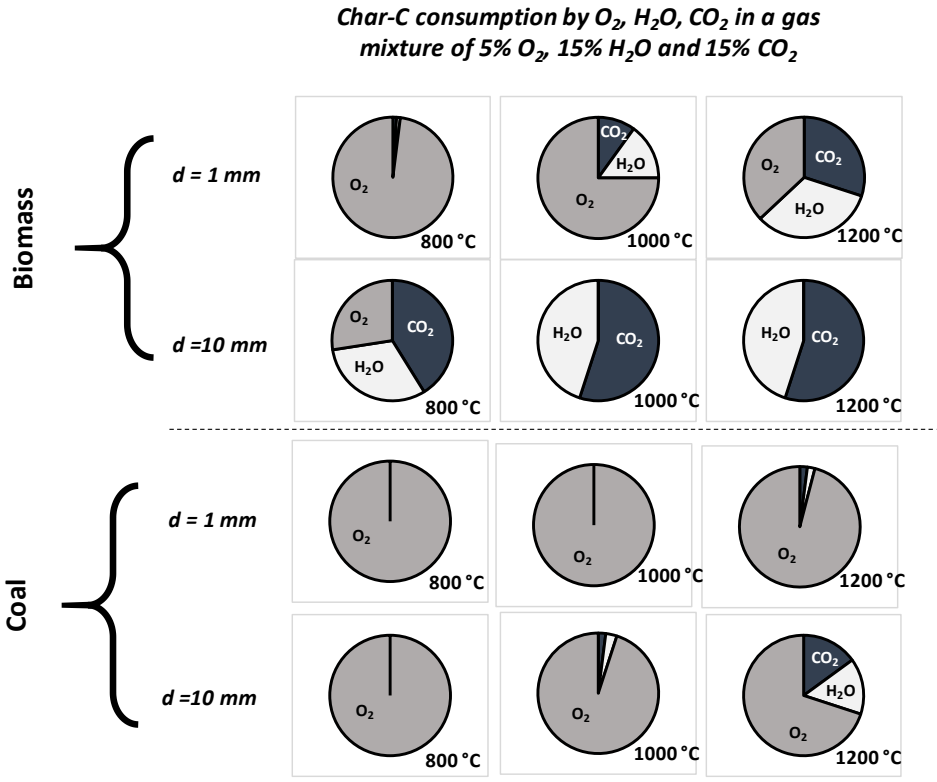

Fig. 7. Computed char consumption by O_2, CO_2 and H_2O under various combustion conditions for biomass and coal.

3.4. Can the CO_2 and H_2O gasification reactions be neglected when predicting char oxidation rates?

Fig. 8 shows experimental char conversion times in O_2, CO_2/H_2O and $O_2/CO_2/H_2O$ at 800, 850 and 900 °C, for 8 and 10 mm char particles. The O_2 concentrations are the same in all cases. The experimental char conversion times are significantly shorter in $O_2/CO_2/H_2O$ than in O_2. This comparison implies that the CO_2 and H_2O reactions play an important role under these conditions. The figure also shows computed times so that the gasification reactions have been neglected, i.e., by setting the pre-exponential factors of the gasification reactions to zero. In

the figure, it can be seen that with this assumption, the computed char oxidation times increase significantly. At 800 °C, i.e., the lowest investigated temperature and the temperature at which the gasification reactions have least significance, the computed char oxidation time increases with a factor of 2 when neglecting the gasification reactions. These experimental char conversion times and computations strongly imply that already at 800 °C, the gasification reactions should be considered to predict char conversions under combustion conditions.

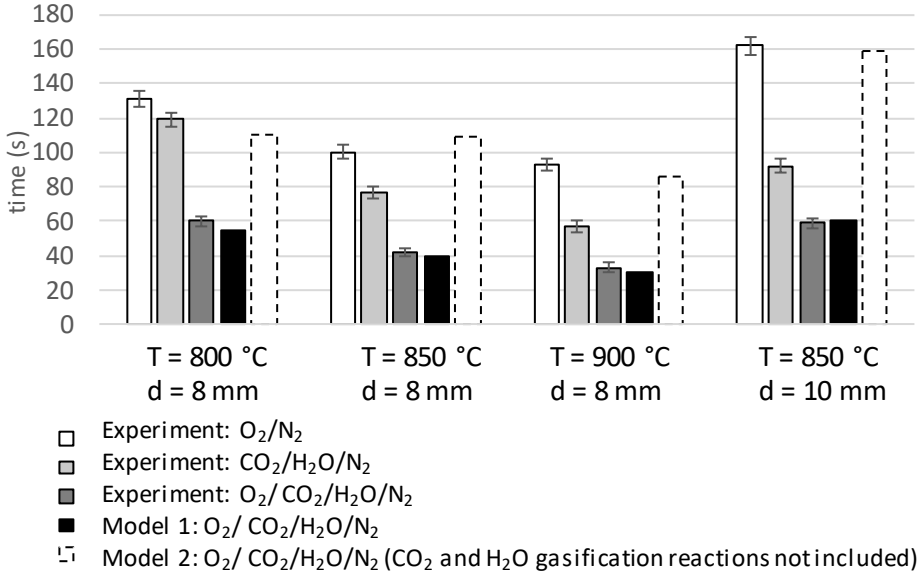

Fig. 8. Experimental and computed char conversion times to 50% of char conversion of 8 and 10 mm char particles at 800, 850 and 900 °C with and without taking into consideration gasification reactions in the computations.

3.5 Char oxidation rates in mixtures based on rates by a single oxidizer

A valid question is whether rates, as given by a single oxidizer, can be combined to give a rate in a mixture of $O_2/CO_2/H_2O/N_2$. In order to validate this hypothesis, the modeled rates in O_2/N_2, CO_2/N_2 and H_2O/N_2 were added with each other and char conversions were determined. Fig. 9 shows char oxidation times in mixtures of $O_2/CO_2/H_2O/N_2$ using the complete model and following the abovementioned hypothesis with the simplified model, i.e., that the rates can be determined based on rates by single oxidizers. The figure shows that the char oxidation times are around 30% shorter using the simplified model. This can be explained by that both CO_2 and H_2O gasification produce high concentrations of CO and H_2 reacting with O_2. This decreases the diffusion of O_2 to the particle surface. As this effect is not accounted for when the rates are determined based on a single oxidizer, the computed and experimental char conversion times are in poor agreement.

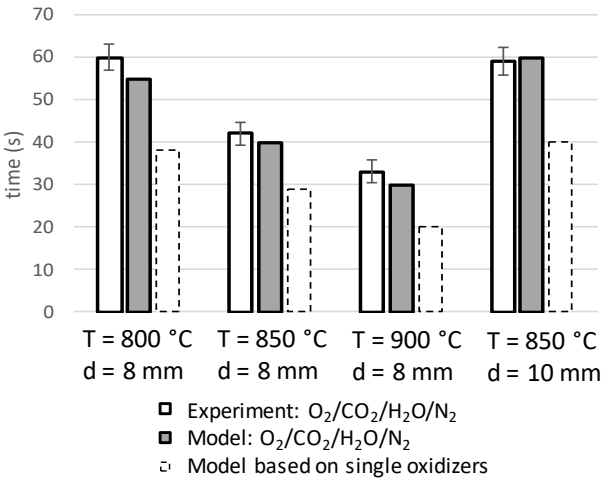

Fig. 9. Experimental and computed char conversion times to 50% of char conversion of 8 and 10 mm char particles at 800, 850 and 900 °C with and without taking into consideration gasification reactions in the computations.

3.6 Implications

In many cases it is useful to design combustion systems using various modeling tools, such as computational fluid dynamics (CFD) modeling. Based on the results of the present study, it is likely that CFD-modeling of biomass combustion will suffer if only char-C reactions with O_2 are taken into consideration, especially if CO_2 and H_2O concentrations are high, which is often the case (see e.g. [35,36]). Results of the present study showed that char oxidation times might be significantly overestimated by neglecting char gasification reactions. In addition, the study showed that a particle model based on single oxidizers may significantly underestimate char conversion times. These findings are important to take into consideration in future CFD-modeling of thermal conversion systems for biomass. For coal chars, simplified single particle models which can be incorporated into CFD-codes have been developed for mixtures in $O_2/CO_2/H_2O/N_2$ [37]. Such CFD-applicable particle models have not yet been developed for biomass, which must be considered in future studies.

4. Conclusions

The study showed that for large particles and high temperatures, gasification reactions by CO_2 and H_2O play a dominant role, while for a sufficiently small particle and low temperature, the O_2 oxidation reaction plays a dominant role in mixtures of $O_2/CO_2/H_2O/N_2$.

In addition, the study showed that char conversion in $O_2/CO_2/H_2O/N_2$ occurred more rapidly than in O_2/N_2 with the same O_2 concentrations in both cases. These results are difficult to explain unless CO_2 and H_2O contributed to char conversion. This has previously not been demonstrated for biomass under well controlled combustion conditions.

Computed char conversions were in good agreement to the experiments under the investigated conditions. It was hypothesized whether oxidation rates in mixtures of $O_2/CO_2/H_2O/N_2$ can be predicted directly based on rates occurring with single oxidizers, i.e.,

without using a detailed model. The results show that the char oxidation rates are overestimated when predicting rates based on single oxidizers, while the detailed model shows a good agreement to the experimental measurement.

Nomenclature

A_{ads} = pre-exponential factor adsorption (1/s)
A_{des} = pre-exponential factor desorption (mol /(s·m^3)
c = concentration (mol/m^3)
c_p = specific heat
D = diffusion coefficient (m^2/s)
E = activation energy (kJ/mol)
$f(X)$ = surface function (-)
f_{min} = least-squares based objective function
H = specific enthalpy of gas species (J/mol)
k_{ads} = kinetic rate constant adsorption (1/s)
k_{des} = kinetic rate constant desorption (mol/(s·m^3)
K = reaction rate constant (mol/(s·m^3))
n = amount (mol)
$\dot{n}$ = molar flow (mol/s)
$\dot{n}'''$ = molar production or consumption rate per unit volume (mol/m^{3}s)
Nu = Nusselt number (-)
Pr = Prandtl number (-)
$\dot{Q}$ = Heat flow (J/s)
r = radial direction (m)
R = universal gas constant (J/molK) and particle radius (m)
Re = Reynolds number (-)
Sc = Schmidt number (-)
Sh = Sherwood number (-)
S = Surface area of sphere (m^2)
T = Temperature (°C or K)
U = velocity of gases
ν = kinematic viscosity (m^2/s)
V = Volume of spherical layer (m^3)
x = molar fraction (-)
X = degree of char conversion (-)
δ = boundary layer thickness (m)
ε = emissivity (-)
λ = thermal conductivity (W/mK)
ρ = density (kg/m^3)
σ = Stefan-Boltzmann constant, 5.67 10^{-8} W/(m^{2}K^4)
Φ = porosity (-)
Ω = stoichiometric ratio (-)

Subscripts
b = backward
C = char carbon
e = external
Eq = *Equilibrium*
expt = experimental
f = forward
h = *heat, thermal*
i = species (O_2, CO_2, H_2O)
j = species (O_2, CO_2,H_2O, CO, H_2)
m = mass, concentration
rad = radiation
p = particle
w = layer in particle
∞ = gas bulk phase

Acknowledgements

This work is part of the project Clean and efficient utilization of demanding fuels (CLUE), with support from the industrial partners: Andritz, Fortum, International Paper, UPM, and Valmet.

References

1. Laurendeau NL. Heterogeneous kinetics of coal char gasification and combustion. Prog. Energy Combust. Sci. 1978;4:221–270.
2. Khitrin LN. Fundamental principles of carbon combustion and factors intensifying the burning of solid fuels. Proc. Combust. Inst. 1957;6:565–573.
3. Stanmore BR, Visona SP. The contribution to char burnout from gasification by H2O and CO2 during pulverized-coal flame combustion. Combust. Flame 1998;113:274–276.
4. Hecht ES, Shaddix CR, Molina A, Haynes BS. Effect of CO2 gasification reaction on oxy-combustion of pulverized coal char. Proceed. Combust. Inst 2011;33:1699–1706.
5. Di Blasi C, Buonanno F, Branca C. Reactivities of some biomass chars in air. Carbon 1999;37:1227–1238.
6. Di Blasi C. Prog. Combustion and gasification rates of lignocellulosic chars. Energy and Combust. Science 2009;35:121–140.
7. Gadsby J, Long FJ, Sleightholm P, Sykes KW. The mechanism of the carbon dioxide-carbon reaction. Proc. Roy. Soc. 1948;193:357–376.
8. Moulijn JA, Kapteijn F. Towards a unified theory of reactions of carbon with oxygen-containing molecules. Carbon 33:1995; 1155–1165.
9. Chen SG, Yang RT, Kapteijn F, Moulijn JA. A new surface oxygen complex on carbon: toward a unified mechanism for carbon gasification reactions. Ind. Eng. Chem. Res. 1993;32:2835–2840.
10. Moulijn JA, Cerfontaine MB, Kapteijn F. Mechanism of the potassium catalysed gasification of carbon in CO2. Fuel 1984;63:1043–1047.
11. Kapteijn F, Moulijn JA. Kinetics of the potassium carbonate-catalysed CO2 gasification of activated carbon. Fuel 1983;62:221–225.
12. Kapteijn F, Peer O, Moulijn JA. Kinetics of the alkali carbonate catalysed gasification of carbon: 1. CO2 gasification. Fuel 1986;65:1371–1376.
13. Mims CA, Pabst JK. Alkali-catalyzed carbon gasification kinetics: Unification of H2O, D2O, and CO2 reactivities. J. Catal. 1987;107:209–220.
14. Dasappa S, Paul PJ, Mukunda HS, Shrinivasa U. Wood-char gasification: experiments and analysis on single particles and packed beds. Proc. Combust. Inst. 1998;27:1335–1342.
15. Goméz-Barea A, Ollero P, Villanueva A. Diffusional Effects in CO2 Gasification Experiments with Single Biomass Char Particles. 2. Theoretical Predictions. Energy Fuels 2006;20:2211–2222.
16. Mermoud F, Golfier F, Salvador S, Van de Steene L, Dirion JL. Experimental and numerical study of steam gasification of a single charcoal particle. Combust. Flame 2006;145:59–79.
17. Paviet F, Bals O, Antonini G. The effects of diffusional resistance on wood char gasification. Process Saf. Environ. Prot. 2008;86:131–140.
18. Park DC, Day SJ, Nelson PF. Nitrogen release during reaction of coal char with O2, CO2 and H2O. Proceedings of the combustion institute 2005;30:2169–2175.
19. Karlström O, Wu H, Glarborg P. Influence of H2O on NO formation during char oxidation of biomass. Fuel 2019;235:1260–1265.

20. Smith IW. The combustion rates of coal chars: A review. Symp (Int) Combustion. 1982;19:1045-1065.
21. Hurt R, Sun J-K, Lunden M. A Kinetic Model of Carbon Burnout in Pulverized Coal Combustion. Combustion and flame 1998;113:181-197.
22. Karlström O, Brink A, Hupa M. Desorption kinetics of CO in char oxidation and gasification in O2, CO2 and H2O. Combust Flame 2015;162:788–96.
23. Howard JB, Williams GC, Fine DH. Kinetics of carbon monoxide oxidation in postflame gases. Symp. Int; Combust. 1973;14:975–986.
24. Jones WP, Lindstedt RP. Global reaction schemes for hydrocarbon combustion. Combust. Flame 1988;73:233–249.
25. Thunman H, Leckner B, Niklasson F, Johnsson F. Combustion of wood particles—a particle model for Eulerian calculations. Combustion and Flame 2002;129:30–46.
26. Satterfield CN. Mass transfer in heterogeneous catalysis, MIT Press, Cambridge, MA (1970)
27. Chen C, Kojima T. Fuel Process Techn. Single char particle combustion at moderate temperature: effects of ash. 1996;47:215–232.
28. Chirone R, Salatino P, Scala F, Solimene R, Urciuolo M. Fluidized bed combustion of pelletized biomass and waste-derived fuels. Combustion and Flame 2008;155:21–36.
29. Karlström O, M. Costa, A. Brink, M. Hupa. CO_2 gasification rates of char particles from torrefied pine shell, olive stones and straw. Fuel 2015;158:753-763.
30. Karlström O, Brink A, Hupa M, Tognotti L. Multivariable optimization of reaction order and kinetic parameters for high temperature oxidation of 10 bituminous coal chars. Combust. Flame 2011;158:2056–2063.
31. Saastamoinen JJ, Kilpinen P, Nordström T. New simplified rate equation for gas-phase CO oxidation at combustion. Energy Fuels 2000;14:1156–1160.
32. Umemoto S, Kajitani S, Hara S. Modeling of coal char gasification in coexistence of CO2 and H2O considering sharing of active sites. Fuel 2013;103:14–21.
33. Guizani C, Escudero Sanz FJ, Salvador S. The gasification reactivity of high-heating-rate chars in single and mixed atmospheres of H2O and CO2. Fuel 2013;108:812–823.
34. Baker RR. Formation of carbon oxides during tobacco combustion: Pyrolysis studies in the presence of isotopic gases to elucidate reaction sequence. Journal of Analytical and Applied Pyrolysis 1983;4:297–334.
35. Hupa M, Karlström O, Vaino E. Biomass combustion technology development–It is all about chemical details. Proceedings Combust Institute 2016;36:113–134.
36. Vainio E, Brink A, Hupa M, Vesala H, Kajolinna T. Fate of Fuel Nitrogen in the Furnace of an Industrial Bubbling Fluidized Bed Boiler during Combustion of Biomass Fuel Mixtures. Energy Fuels 2012;26:94–101.
37. Geier M, Shaddix CR, Davis KA, Shim HS. On the use of single-film models to describe the oxy-fuel combustion of pulverized coal char. Applied Energy 2012;93:675–679.